Applied Physics Letters

Fully transparent GaN homojunction tunnel junction-enabled cascaded blue LEDs

Cite as: Appl. Phys. Lett. **117**, 051103 (2020); https://doi.org/10.1063/5.0015403
Submitted: 27 May 2020 . Accepted: 23 July 2020 . Published Online: 04 August 2020

Zane Jamal-Eddine, Syed M. N. Hasan, Brendan Gunning, Hareesh Chandrasekar, Mary Crawford, Andrew Armstrong, Shamsul Arafin, and Siddharth Rajan

Fully transparent GaN homojunction tunnel junction-enabled cascaded blue LEDs

Cite as: Appl. Phys. Lett. **117**, 051103 (2020); doi: 10.1063/5.0015403
Submitted: 27 May 2020 · Accepted: 23 July 2020 ·
Published Online: 4 August 2020

View Online Export Citation CrossMark

Zane Jamal-Eddine,[1,a)] Syed M. N. Hasan,[1] Brendan Gunning,[2] Hareesh Chandrasekar,[1] Mary Crawford,[2] Andrew Armstrong,[2] Shamsul Arafin,[1] and Siddharth Rajan[1,3]

AFFILIATIONS

[1]Department of Electrical and Computer Engineering, The Ohio State University, Columbus, Ohio 43210, USA
[2]Sandia National Laboratories, Albuquerque, New Mexico 87185, USA
[3]Department of Materials Science and Engineering, The Ohio State University, Columbus, Ohio 43210, USA

[a)]Author to whom correspondence should be addressed: jamal-eddine.1@osu.edu

ABSTRACT

A sidewall activation process was optimized for buried magnesium-doped p-GaN layers yielding a significant reduction in tunnel junction-enabled light emitting diode (LED) forward voltage. This buried activation enabled the realization of cascaded blue LEDs with fully transparent GaN homojunction tunnel junctions. The initial optimization of buried p-GaN activation was performed on PN junctions grown by metal organic chemical vapor deposition (MOCVD) buried under hybrid tunnel junctions grown by MOCVD and molecular beam epitaxy. Next the activation process was implemented in cascaded blue LEDs emitting at 450 nm, which were enabled by fully transparent GaN homojunction tunnel junctions. The tunnel junction-enabled multi-active region blue LEDs were grown monolithically by MOCVD. This work demonstrates a state-of-the-art tunnel junction-enabled cascaded LED utilizing homojunction tunnel junctions which do not contain any heterojunction interface.

In recent years much interest has been generated in the study of tunnel junction-enabled III-Nitride optoelectronics. There has been significant research on tunnel junctions (TJs) grown by molecular beam epitaxy (MBE),[1–6] metal organic chemical vapor deposition (MOCVD),[7–15] and Hybrid (MOCVD+MBE) growth.[16–18] Tunnel junctions have been explored for a wide variety of applications such as efficient current spreading without the use of absorbing indium tin oxide (ITO) contacts to p-type GaN,[19,20] for efficient hole injection into ultraviolet light emitting diode (UVLED) multiple-quantum well (MQW) active regions,[21–23] and even the cascading of multiple LED active regions.[24–26] Recently it has also been shown that tunnel junctions can be utilized to cascade multiple laser active regions.[27] Tunnel junction-enabled cascaded LED structures have also been utilized to fabricate dual-wavelength LEDs,[28–30] and have been discussed as a possible solution for overcoming the efficiency droop phenomenon native to III-Nitride based LEDs.

Previously multi-active region III-Nitride LEDs were reported by Chang *et al.* with tunnel junctions based on GaN/InGaN/GaN polarization-engineered heterojunctions, with external quantum efficiency (EQE) up to 71.3%.[25] Later Chang *et al.* reported multi-active region III-Nitride LEDs with tunnel junctions based on GaN/InGaN/AlN/InGaN/GaN polarization-engineered heterojunctions, with EQE up to 93%.[26] However, the devices in both studies showed a significant voltage penalty across each tunnel junction within the structures. Also, the use of InGaN may lead to issues such as absorption in the tunnel junction layers and issues with the thermal budget during growth. In this work, we describe the demonstration of multi-active region LEDs with transparent GaN homojunction tunnel junctions.

One of the key challenges for multi-active region structures is the activation of buried p-GaN layers. Previous work on such structures by Kuwano *et al.* demonstrated activation of buried p-layers was feasible under an optimized activation condition of 725 C in dry air for 30 min.[31] With the goal of reducing the voltage penalty in our GaN homojunction we studied the forward voltage of NPN structures activated under various buried p-GaN activation conditions. We found that activation performed at 900 C in N_2 ambient resulted in a 300 mV reduction in forward voltage for our NPN structures as compared to the previously reported optimal condition of 725 C in dry air. These results are discussed in greater detail below.

Li *et al.* performed a further study of buried p-GaN activation by metric of breakdown voltage in MOCVD grown GaN verticle devices.[32] Studying the previously reported optimized activation condition Li *et al.* have shown that the device with the highest breakdown voltage corresponded to a lower bound of Mg activation equal to 28%. One point mentioned by Li *et al.* was that higher p-type doping concentrations in buried p-GaN layers may lead to higher Mg activation efficiency by means of increasing the diffusion length of Hydrogen. In this work, we show that Mg activation conditions used to activate p-type GaN through the c-plane surface may not be optimal for sidewall activation, such as that required for multiple active region LEDs. Using optimized activation conditions for sidewalls, we can greatly reduce the voltage drop across the tunnel junctions. We use the optimized activation conditions to demonstrate all-MOCVD homojunction tunnel junction based multiple-active region LEDs.

All MOCVD growth in this report was performed at atmospheric pressure in a Taiyo Nippon Sanso SR4000HT reactor. The substrates were $\sim$6 μm thick n-type GaN/sapphire c-plane templates with typical dislocation density of $\sim 10^8\,\mathrm{cm}^{-2}$. For the PN junction structures, the n-type layers were grown at 1050 °C while the p-type layers were grown at 1015 °C. For the LED structures, the InGaN underlayer was grown at 900 °C and the MQW active region was grown at $\sim$810 °C. The tunnel junction layers, including the $\sim$500 nm thick n-GaN layer, were grown at reduced temperatures (compared to the PN junctions) of 900–975 °C in order to reduce thermal budget and limit degradation of the underlying MQW active region(s) which is of particular importance for the multi-junction cascaded LEDs. Previous study on tunnel junction design revealed that maximizing both [Si] and [Mg] doping concentrations in the heavily doped tunnel junction layers would yield the lowest tunnel junction resistance. The doping concentrations within the tunnel junction were chosen to be the maximum value possible by MOCVD growth while still maintaining good material quality in subsequently grown layers. As such we chose [Si]$= 3.5 \times 10^{20}\,\mathrm{cm}^{-3}$ and [Mg]$= 2 \times 10^{20}\,\mathrm{cm}^{-3}$ for the n-type and p-type tunnel junction layers, respectively.

Two separate experiments are described here. For optimization of activation conditions, PN junction structures were used [Fig. 1(a)]. Test structures were fabricated starting with mesa-isolation of the device structure by Inductively Coupled Plasma-Reactive Ion Etching (ICP-RIE) etching followed by activation of buried p-GaN layers in a rapid thermal anneal system (details are discussed later in this paper). Ti/Al/Ni/Au bottom contact was evaporated and annealed for 30 s at 850 °C in N_2 ambient. Ring-shaped Al/Ni/Au top n-type contacts were deposited to study the optical emission uniformity.

Various activation conditions were studied on the buried MOCVD grown p-GaN layers within the structure, including those reported previously by Kuwano *et al.*[31] Activation at 725 °C in dry air was tested for 30, 40, and 50 minutes. Activation was also tested in N_2 ambient at 725 °C for 40 min and at 900 °C for 12 min. To test multiple active region LEDs, two separate device structures were grown. Sample LED1 and LED2 had one and two active regions, respectively [Fig. 1(c)]. The LED device structures were fabricated starting with mesa-isolation of the device structure by ICP-RIE etching followed by activation of buried p-GaN layers under optimized conditions (discussed below). Ti/Al/Ni/Au bottom contact was evaporated and annealed for 30 s at 850 °C. Ring-shaped Al/Ni/Au top n-type contacts were deposited to study the optical emission uniformity.

The different activation conditions were compared by merit of forward voltage and uniformity of optical emission from the surface. Figure 2(a) shows a plot of the measured current density as a function

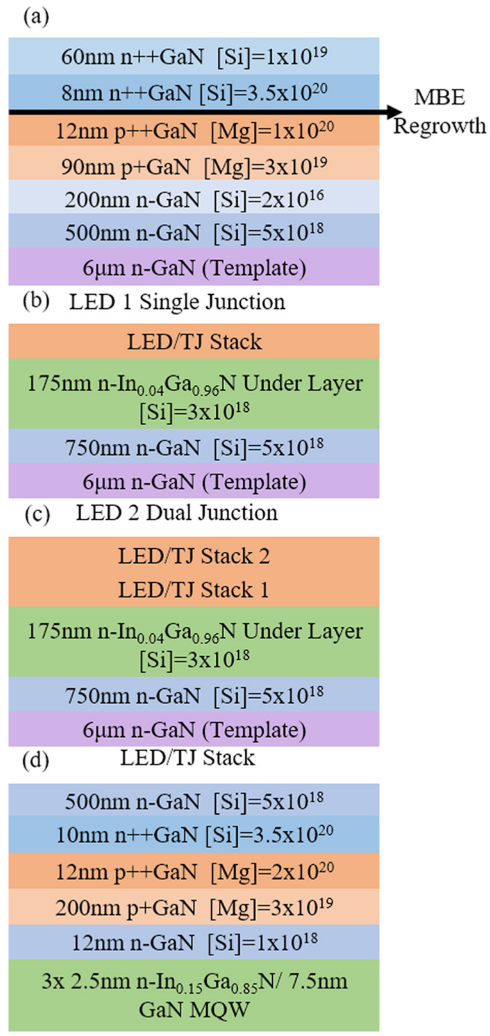

FIG. 1. The epitaxial structure of (a) the pn-junction tunnel junction devices used in the optimization of the buried p-GaN activation condition, (b) LED1, the single junction LED/TJ device, (c) LED2, the dual junction (2×) LED/TJ device, and (d) the detailed epitaxial layers of the LED/TJ stack.

of forward voltage for the various activation conditions tested. It is worth noting that the MOCVD growth took place on one wafer, which was then diced into smaller samples. These smaller samples were all co-loaded for one MBE regrowth. Thus, the variation in forward voltage between samples should be attributed to the different activation condition performed on each sample. The total differential resistance of each device measured at 1 kA/cm^2 is plotted in Fig. 2(b).

The uniformity of optical emission from the sample surfaces was also studied. An optical micrograph showing uniform emission from the sample activated at 900 °C for 12 min in N_2 ambient is shown in the inset of Fig. 2(a). The activation completed at 900 °C in N_2 ambient for 12 min resulted in the lowest turn-on voltage and the most uniform electroluminescence. The forward voltage at 100 A/cm^2 was 0.54 V lower for this sample (900 °C/12 min/N_2) as compared to the

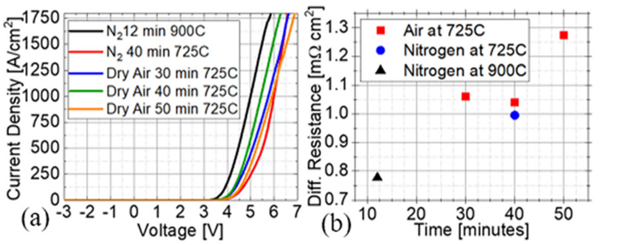

FIG. 2. (a) The current density vs voltage characteristics for the various buried p-GaN activation conditions tested. (b) The overall differential resistance measured at a driving current of 1 kA/cm^2 for each activation condition tested.

sample activated in dry air at 725 °C for 30 min (the optimized condition previously reported by Kuwano *et al.*[31]).

The optimized activation condition for MOCVD grown buried p-GaN was utilized to fabricate all-MOCVD homojunction tunnel junction based multiple-active region LEDs as described previously. These devices were characterized both electrically and optically, and the efficacy of utilizing fully transparent GaN-based homojunction tunnel junctions for a cascaded LED structure was evaluated. As can be seen in the current density vs voltage characteristics shown in Fig. 3(a) the forward voltage at a driving current density 35 A/cm^2 scales by a factor of 2.08 between LED1 (V_F = 4.4 V at 35 A/cm^2) and LED2 (V_F = 9.15 V at 35 A/cm^2). Our single junction device LED1 shows a significantly higher forward voltage than that of a state-of-the-art blue LED. State-of-the-art blue LEDs have reached wall-plug-efficiencies (WPE) greater than 80% according to the U.S. Department of Energy solid state lighting research and development opportunities plan.[33] Kimura *et al.* reported a blue LED emitting at 437 nm with a peak WPE of 84% which had a forward voltage of 3.31 V at 35 A/cm^2 and an on-resistance of 2.6 Ohms.[34] In comparison, our single junction device LED1 had a forward votlage of 4.4 V at 35 A/cm^2 and an on-resistance of 0.1 Ohms. The lower on-resistance of our LED may be attributed to the increased efficiency of the tunnel junction at high current densities as compared to that of a conventional p-GaN contact. The large increase in forward voltage between our single junction device LED 1 and that of a state-of-the-art conventional blue LED is attributed to two factors. The first factor being that the LED structure within the device has not been optimized. We have not focused on optimizing the forward voltage of the LED emitter itself beccause the purpose of this work is to demonstrate the viability of a fully transparent GaN homojunction for application in cascaded LED device structures. Optimization of quantum well design, doping concentrations, and layer thicknesses within the LED could all lead to a substantial decrease in the forward voltage of LED1. Furthermore, the tunnel junction in our single junction device LED1 adds an extra voltage penalty which contributes to an increase in the measured forward voltage. Although we have shown that it is possible to reduce this tunnel junction voltage penalty to the point where it is of interest for applications in cascaded LED structures, it still contributes to an increase in forward voltage for the device.

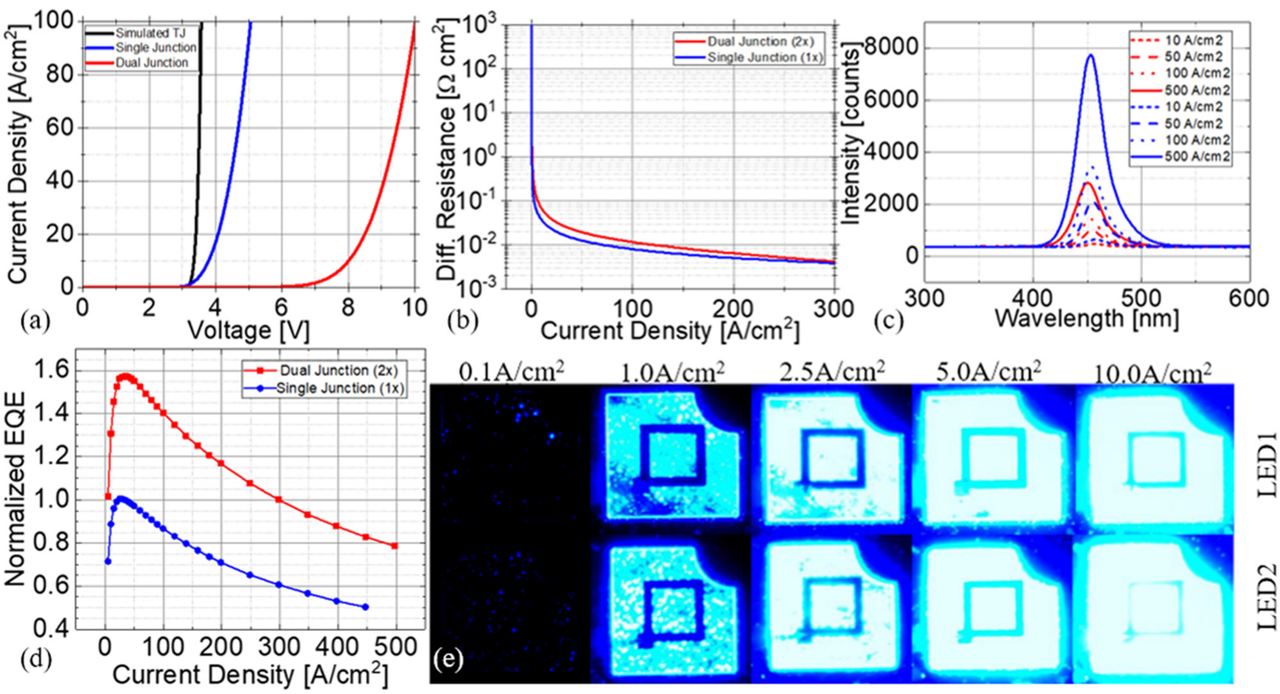

FIG. 3. (a) The current density vs voltage characteristics for LED1 and LED2 are shown in blue and red, respectively. The black curve depicts the current density vs voltage for a simulated GaN homojunction with nominal doping values of the tunnel junction in LED1. (b) The overall differential resistance vs current density for LED1 and LED2. (c) The electroluminescence spectra measured for LED1 (blue), and LED2 (red). Peak emission wavelength did not change between LED1 and LED2. (d) The EQE measurement as a function of driving current density. The peak EQE of LED2 scaled by a factor of 1.6 as compared with that of LED1. (e) Optical micrographs of emission uniformity for LED1 and LED2 at current densities between 0.1 A/cm^2 and 10.0 A/cm^2.

It is worth noting that the GaN homojunction tunnel junction simulated with the same nominal doping concentrations as the experimental tunnel junction in LED1 shows a lower voltage drop than that measured in LED1. This discrepency has a few possible origins. First, the LED structures in this study have not been optimized. As discussed above, they may display higher-than-expected forward voltage for a LED emitting at 450 nm. Second the mismatch between simulation and measurement could be due to issues faced with Mg doping in MOCVD growth of GaN. The memory effect causes non-optimal Mg doping profiles in the p++ layer of the GaN homojunction tunnel junction.[12] Secondary ion mass spectrometry (SIMS) analysis (not shown here) suggests the Mg concentration in the p++ layer of the homojunction peaks at a lower than nominal value and, due to the Mg memory effect in MOCVD, the Mg concentration tails off into the n++ region of the tunnel junction. The comparison with simulation shows the necessity for further study of the GaN homojunction tunnel junction, and specifically the relationship between tunnel junction voltage penalty and the Mg doping concentration and profile within the p++ layer. The aforementioned study is under way and will be reported at a later time. Figure 3(b) shows the measured overall differential resistance for LED1 and LED2 as a function of current density. The overall differential resistance is greater than a factor of two larger for LED2 as compared to LED1 in the current regime of peak efficiency (10 A/cm^2–100 A/cm^2). As the current density is increased further (above 200 A/cm^2) the overall differential resistance for LED1 and LED2 becomes similar, possibly due to increased tunnel junction efficiency at higher operating current density.

LED1 and LED2 were evaluated from an optical standpoint both qualitatively and quantitatively. Optical micrographs of devices with mesa size of 105 μm $\times$ 105 μm operating at driving currents between 0.1 A/cm^2 and 10 A/cm^2 were captured to compare the uniformity of emission. The images confirm that the devices were activated all the way through the center of the device after sidewall activation of the buried p-GaN layers. The devices show emission of the same intensity in the center of the device as compared to the edges [Fig. 3(e)], indicating uniform Mg activation throughout the device mesa from the center to the sidewall. Optical micrographs at a driving current of 0.1 A/cm^2 show spots of "early" luminescence which we postulate may be areas where the tunnel junction resistance is lower due to non-uniformity in growth. Quantitative optical measurements of electroluminescence (EL) spectra and External Quantum Efficiency (EQE) were also performed. Figure 3(c) shows the results of the EL measurements for both LED1 and LED2. The measurement was performed using a linear silicon CCD array detector based spectrometer fitted with a cosine corrector to increase the collection field of view. The probe was positioned above each sample manually for each measurement and replication of the same geometry between subsequent measurements was difficult, as such, the intensities of the EL spectra should not be compared quantitatively. The measurement is accurate for determining the peak wavelength of the EL spectra, and, as shown in Fig. 3(c), the introduction of the second junction did not shift the peak EL wavelength. Both LED1 and LED2 show peak emission wavelengths of $\lambda = 450$–452 nm as the current densities are varied from 10 A/cm^2 to 500 A/cm^2.

The EQE of each device was calculated by measuring the optical output power with a Thorlabs PM100D optical power meter fitted with a S120VC photodiode power sensor. The multi-active region LED devices were placed directly on top of the photodiode power sensor, and probed for electrical contact from the top. All light was collected from the backside of the sample through the sapphire substrate. The measurements performed may significantly underestimate the output power as the measurements are done on-wafer without any device packaging. Nonetheless, we still gain useful information about the EQE scaling factor from these on wafer measurements, the results of which are shown in Fig. 3(d). The EQE measurements have been normalized to the peak EQE value of LED1, the single junction sample, for ease of interpretation. The EQE of LED2 scaled by a factor of 1.6 as compared with LED1. This 60% increase in EQE with the addition of the second active region in the cascaded structure is state-of-the-art for a cascaded LED device based on fully transparent GaN homojunction tunnel junctions.

There are a few factors which may be responsible for the EQE of LED2 not scaling directly with the number of junctions (2). The first reason is related to the on wafer measurement setup discussed earlier. As the device mesa height changes between LED1 and LED2, the geometry of the mesa, and thus the light extraction efficiency also changes. This could lead to less light being captured in the photodiode power sensor on the backside of the sample. Another factor one must consider is the possibility of the degradation of the active regions grown earlier in the cascaded LED structure, as the subsequent LEDs are grown. This effect would be more pronounced as more LEDs are added into the cascaded structure. Although this effect has not yet been measured or quantified, it cannot be disqualified until further study is completed and could be a critical limiting factor in the growth of multi-junction LEDs.

This study investigated the effect that activation of Mg dopants in buried MOCVD grown layers can have on the forward voltage of tunnel junction-enabled multi-active region LED devices. We have shown that it is possible to achieve a significant reduction in the forward voltage of cascaded multi-active region LED structures when the buried p-GaN activation condition is carefully optimized. We also demonstrate the achievement of forward voltage scaling that is close to the number of junctions in the cascaded LED structure, even though the tunnel junctions do not utilize InGaN interlayer heterojunctions for the added benefit of polarization engineering. This work demonstrates a state-of-the-art increase in EQE of 60% between the single and dual junction LED structure for a cascaded LED utilizing a fully transparent GaN homojunction tunnel junction. We show that it is possible to achieve significant EQE scaling, and low nearly linear voltage scaling in cascaded LED structures utilizing even the most simple tunnel junction design.

Continued optimization of the magnesium activation process is under way and we have observed further reduction of the tunnel junction voltage loss which will be published separately. The effect of the possible degradation of buried LED active regions during the growth of the cascaded LED structures must still be investigated.

Ultimately, this work shows promise for the prospect of utilizing tunnel junction-enabled multi-active region cascaded LED structures to circumvent efficiency droop phenomenon in visible emitters. With continued optimization of buried p-GaN activation, tunnel junction design, and growth of the multi-active region LEDs, the voltage dropped across the devices can be reduced further. By reducing the voltage dropped across each tunnel junction beyond the values reported here the wall plug efficiency scaling can be improved significantly for future tunnel junction-enabled multi-active region cascaded

LED device structures. These structures may one day find application in circumventing the efficiency droop and enabling significantly more efficient high output power lighting applications for LEDs.

This material is based upon work supported by the U.S. Department of Energy's Office of Energy Efficiency and Renewable Energy (EERE) under the Building Technologies Office (BTO) Award No. 31150. Sandia National Laboratories is a multi-mission laboratory managed and operated by National Technology and Engineering Solutions of Sandia, LLC., a wholly owned subsidiary of Honeywell International, Inc., for the U.S. Department of Energy's National Nuclear Security Administration under Contract No. DE-NA-0003525. The views expressed in the article do not necessarily represent the views of the U.S. Department of Energy or the United States Government.

DATA AVAILABILITY

The data that support the findings of this study are available from the corresponding author upon reasonable request.

REFERENCES

[1]J. Simon, Z. Zhang, K. Goodman, H. Xing, T. Kosel, P. Fay, and D. Jena, Phys. Rev. Lett. **103**(2), 026801 (2009).
[2]S. Krishnamoorthy, F. Akyol, and S. Rajan, Appl. Phys. Lett. **105**(14), 141104 (2014).
[3]M. Malinverni, D. Martin, and N. Grandjean, Appl. Phys. Lett. **107**(5), 051107 (2015).
[4]F. Akyol, S. Krishnamoorthy, Y. Zhang, J. Johnson, J. Hwang, and S. Rajan, Appl. Phys. Lett. **108**(13), 131103 (2016).
[5]B. P. Yonkee, E. C. Young, C. Lee, J. T. Leonard, S. P. DenBaars, J. S. Speck, and S. Nakamura, Opt. Express **24**(7), 7816 (2016).
[6]E. A. Clinton, E. Vadiee, S.-C. Shen, K. Mehta, P. D. Yoder, and W. A. Doolittle, Appl. Phys. Lett. **112**(25), 252103 (2018).
[7]M. Kaga, T. Morita, Y. Kuwano, K. Yamashita, K. Yagi, M. Iwaya, T. Takeuchi, S. Kamiyama, and I. Akasaki, Jpn. J. Appl. Phys., Part 1 **52**(8S), 08JH06 (2013).
[8]D. Hwang, A. J. Mughal, M. S. Wong, A. I. Alhassan, S. Nakamura, and S. P. DenBaars, Appl. Phys. Express **11**(1), 012102 (2018).
[9]S. Neugebauer, M. P. Hoffmann, H. Witte, J. Bläsing, A. Dadgar, A. Strittmatter, T. Niermann, M. Narodovitch, and M. Lehmann, Appl. Phys. Lett. **110**(10), 102104 (2017).
[10]S. Lee, C. A. Forman, C. Lee, J. Kearns, E. C. Young, J. T. Leonard, D. A. Cohen, J. S. Speck, S. Nakamura, and S. P. DenBaars, Appl. Phys. Express **11**(6), 062703 (2018).
[11]P. Sohi, M. Mosca, Y. Chen, J.-F. Carlin, and N. Grandjean, Semicond. Sci. Technol. **34**, 015002 (2019).
[12]Y. Akatsuka, S. Iwayama, T. Takeuchi, S. Kamiyama, M. Iwaya, and I. Akasaki, Appl. Phys. Express **12**(2), 025502 (2019).
[13]V. Fan Arcara, B. Damilano, G. Feuillet, A. Courville, S. Chenot, and J.-Y. Duboz, AIP Adv. **9**(5), 055101 (2019).
[14]D. Minamikawa, M. Ino, S. Kawai, T. Takeuchi, S. Kamiyama, M. Iwaya, and I. Akasaki, Phys. Status Solidi B **252**(5), 1127 (2015).
[15]D. Takasuka, Y. Akatsuka, M. Ino, N. Koide, T. Takeuchi, M. Iwaya, S. Kamiyama, and I. Akasaki, Appl. Phys. Express **9**(8), 081005 (2016).
[16]E. C. Young, B. P. Yonkee, F. Wu, S. H. Oh, S. P. DenBaars, S. Nakamura, and J. S. Speck, Appl. Phys. Express **9**(2), 022102 (2016).
[17]A. I. Alhassan, E. C. Young, A. Y. Alyamani, A. Albadri, S. Nakamura, S. P. DenBaars, and J. S. Speck, Appl. Phys. Express **11**(4), 042101 (2018).
[18]K. W. Hamdy, E. C. Young, A. I. Alhassan, D. L. Becerra, S. P. DenBaars, J. S. Speck, and S. Nakamura, Opt. Express **27**(6), 8327 (2019).
[19]S.-R. Jeon, Y.-H. Song, H.-J. Jang, G. M. Yang, S. W. Hwang, and S. J. Son, Appl. Phys. Lett. **78**(21), 3265 (2001).
[20]T. Takeuchi, G. Hasnain, S. Corzine, M. Hueschen, Jr., R. P. Schneider, C. Kocot, M. Blomqvist, Y-L. Chang, D. Lefforge, M. R. Krames, L. W. Cook, and S. A. Stockman, Jpn. J. Appl. Phys., Part 2 **40**, L861 (2001).
[21]Y. Zhang, S. Krishnamoorthy, F. Akyol, S. Bajaj, A. A. Allerman, M. W. Moseley, A. M. Armstrong, and S. Rajan, Appl. Phys. Lett. **110**(20), 201102 (2017).
[22]Y. Zhang, Z. Jamal-Eddine, F. Akyol, S. Bajaj, J. M. Johnson, G. Calderon, A. A. Allerman, M. W. Moseley, A. M. Armstrong, J. Hwang, and S. Rajan, Appl. Phys. Lett. **112**(7), 071107 (2018).
[23]C. Kuhn, L. Sulmoni, M. Guttmann, J. Glaab, N. Susilo, T. Wernicke, M. Weyers, and M. Kneissl, Photonics Res. **7**(5), B7 (2019).
[24]F. Akyol, S. Krishnamoorthy, Y. Zhang, and S. Rajan, Appl. Phys. Express **8**(8), 082103 (2015).
[25]S. Chang, W. Lin, and C. Yu, IEEE Electron Device Lett. **36**(4), 366 (2015).
[26]S. Chang, W. Lin, and W. Chen, IEEE J. Quantum Electron. **51**(8), 3300505 (2015).
[27]M. Siekacz, G. Muziol, M. Hajdel, M. Żak, K. Nowakowski-Szkudlarek, H. Turski, M. Sawicka, P. Wolny, A. Feduniewicz-Żmuda, S. Stanczyk, J. Moneta, and C. Skierbiszewski, Opt. Express **27**(4), 5784 (2019).
[28]I. Ozden, E. Makarona, A. V. Nurmikko, T. Takeuchi, and M. Krames, Appl. Phys. Lett. **79**(16), 2532 (2001).
[29]C. H. Chen, S. J. Chang, Y. K. Su, J. K. Sheu, J. F. Chen, C. H. Kuo, and Y. C. Lin, IEEE Photonics Technol. Lett. **14**(7), 908 (2002).
[30]M. J. Grundmann and U. K. Mishra, Phys. Status Solidi C **4**(7), 2830 (2007).
[31]Y. Kuwano, M. Kaga, T. Morita, K. Yamashita, K. Yagi, M. Iwaya, T. Takeuchi, S. Kamiyama, and I. Akasaki, Jpn. J. Appl. Phys., Part 1 **52**(8S), 08JK12 (2013).
[32]W. Li, K. Nomoto, K. Lee, S. M. Islam, Z. Hu, M. Zhu, X. Gao, J. Xie, M. Pilla, D. Jena, and H. G. Xing, Appl. Phys. Lett. **113**(6), 062105 (2018).
[33]U.S. Department of Energy, *Solid-State Lighting R&D Plan* (U.S. Department of Energy, 2016).
[34]S. Kimura, H. Yoshida, K. Uesugi, T. Ito, A. Okada, and S. Nunoue, J. Appl. Phys. **120**(11), 113104 (2016).